

Perfect photon indistinguishability from a set of dissipative quantum emitters

J.GUIMBAO*¹, L.SANCHIS¹, L.M.WEITUSCHAT¹, J.M. LLORENS¹, P.A.POSTIGO^{1,2}

¹*Instituto de Micro y Nanotecnología, INM-CNM, CSIC (CEI UAM+CSIC) Isaac Newton, 8, E-28760, Tres Cantos, Madrid, Spain*

²*The Institute of Optics, University of Rochester, Rochester, New York 14627, USA*

*j.guimbao@csic.es

Abstract: Single photon sources (SPS) based on semiconductor quantum dot (QD) platforms are restricted to low temperature (T) operation due to the presence of strong dephasing processes. Despite the integration of QD in optical cavities provides an enhancement of its emission properties, the technical requirements for maintaining high indistinguishability (I) at high T are beyond the state of the art. Recently, new theoretical approaches have shown promising results by implementing two-dipole-coupled-emitter systems. Here, we have developed a theory to estimate I in a two-emitter system with strong dephasing coupled to a photonic cavity. We have obtained an analytical expression for I that predicts the cavity restrictions depending on the distance between the emitters. Furthermore, we develop an alternative interpretation of I which provide insights for systems with a larger number of emitters. We find the optimal configuration for maximum I in the case of a five-emitter system using a machine-learning optimization procedure which models the Lindblad equation and provides the optimal position of each emitter to maximize I . The optimized configuration provides perfect I while relaxes the cavity requirements to more experimentally accessible values.

Introduction

Over the last decade, milestones achieved in integrated quantum photonics (IQP) have shown promising results. While other quantum technologies (QT) like ion trapping or superconducting systems demonstrated its first logic operation in the 1990s^{1,2}, the first IQP gate wasn't developed until 2008³. Yet, despite its immaturity, IQP has become established in a wide range of proposed schemes like Quantum Communications^{4,5}, Quantum Computation⁶, Quantum Simulation⁷ and Quantum Metrology⁸. In this context, IQP is showing a new leading candidate for the future q-bit in QT: the indistinguishable single photon.

A suitable platform for indistinguishable SPS are epitaxially grown semiconductor QDs. QDs enable site control during growth⁹ and the possibility of monolithic integration inside photonic nanocavities^{10,11},

providing enhanced quantum emission. As a result, many recent experimental demonstrations have reported record I with cavity-integrated QDs at cryogenic T ^{12,13,14}. However, for T above the cryogenic regime QDs are subject to pure dephasing mechanisms which reduce the coherence of the emission^{15,16,17}. As a consequence, I reduces to non-practical values for quantum information tasks^{18,19,20,21,22}. In an attempt to overcome this limitation, there is a variety of cavity-engineering approaches^{23,24}. However, several theoretical works^{25,26,27} show that cavity quality factors (Q) above 4×10^7 are needed for QDs at room T , while, to date, the highest reported Q coupled to a quantum emitter is about $Q = 55000$ ²⁸. In this regard, the theoretical exploration over new strategies for enhancing I in the presence of dephasing processes is especially relevant.

Recently, theoretical studies^{29,30,31,32,33} have shown that the enhancement and tunability of single photon emission is possible through interfaces based on two-emitter systems coupled to a cavity mode. In their scheme, tunable bandwidth and Purcell enhancement are achieved by dynamical control of the collective states of the two emitters coupled by dipolar interaction. The results offer interesting possibilities for application in single photon generation for quantum information processing. At the same time, deterministic positioning required for dipole-dipole coupling between emitters have been experimentally demonstrated with several SPS platforms: organic molecules³⁴, color centers in h-BN³⁵ and diamond³⁶, terylene molecules³⁷ and QDs^{38,39,40,41}. The potential applications of this cluster systems for the enhancement of I have not been studied neither theoretically or experimentally. As we will show, the cooperative dynamics of these cluster systems can be exploited to maintain high I with arbitrary low Q cavities by tuning the energy transfer rates between the emitters.

In this work we have developed a theory for the estimation of I in a two-emitter system with strong dephasing coupled to a single-mode cavity. We have derived an analytical expression of I as a function of the distance between the emitters, cavity decay rate, and pure dephasing rate. The results show how the requirements of the cavity for high I change with the strength of the dipolar interaction. Taking the model further, we propose a new interpretation of the I value which allows us to estimate its behavior with larger systems (i.e. systems with more than two emitters). We have performed numerical simulations of a system of five dipole-coupled emitters to find the optimal configuration for maximum I . For the optimization process we have developed a novel machine-learning (ML) scheme based on a hybrid neural network (NN)-genetic algorithm (GA) to find the position of each emitter to maximize I . The

optimization procedure provides perfect I (i.e., $I = 1$) in arbitrary low Q cavities, offering unprecedented advantages for relaxing the cavity requirements and favoring the use of QDs as SPS at room T.

Results

INDISTINGUISHABILITY OF DIPOLE-COUPLED EMITTERS

We consider a system of two quantum emitters (QE) coupled to a single-mode cavity field. Each QE is described by a Two-Level-System $\{|g\rangle, |e\rangle\}$ with a decay rate γ and a pure dephasing rate γ^* . The QEs interact with each other by direct dipole-dipole coupling with a strength $\Omega_{12} = \frac{3\gamma}{4(kd)^3}$, where k is the wave vector of the emission and d is the distance between the QEs²⁹. The cavity field in the Fock basis $\{|0\rangle, |1\rangle\}$ has a decay rate κ and is coupled to the QEs with a coupling constant g . Assuming $kd \ll 1$ and no detuning between the Qes this system is equivalent to a single effective QE $\{|gg\rangle, |+\rangle\}$ (e-QE) with a decay rate 2γ ²⁹ (see Fig 1.a). Here $|+\rangle$ represents the superradiant state $|+\rangle = \frac{|eg\rangle - |ge\rangle}{\sqrt{2}}$. The e-QE is coupled to the cavity field with $\sqrt{2}g$ and a cavity detuning $\delta = \Omega_{12}$ ³⁰. In Fig 1.b, c we report the numerical calculation of I for the e-QE as a function of the cavity parameters (g and κ) for fixed d , γ and $\gamma^* = 10^4\gamma$. Fig 1.b shows the region of high I in the incoherent regime (i.e. $g \ll \kappa + \gamma + \gamma^*$) while Fig 1.c corresponds to the region in the coherent regime ($g \gg \kappa + \gamma + \gamma^*$).

Within the incoherent regime the dynamics can be approximated to a population transfer between the e-QE and the cavity field with an effective transfer rate R ²⁵. From the non-equilibrium Green's function (ne-G) of the system we obtain (see methods):

$$R = \frac{4g^2\Gamma}{\Gamma^2 + \frac{\gamma^2}{(kd)^6}}, \quad I = \frac{\gamma\kappa[\Gamma^3 + \Omega_{12}] + [4g^2(\gamma+1) + \Omega_{12}\frac{\kappa\gamma}{\Gamma}] \cdot [\Gamma^2 + \Omega_{12}]}{[\Gamma^2 + \Omega_{12} + 8g^2] \cdot [\kappa\Gamma^2 + \Omega_{12} + 4g^2\Gamma]} \quad (1)$$

Where $\Gamma = \gamma + \gamma^* + \kappa$. In this regime the cavity behaves as an effective emitter pumped by the e-QE, and the conditions for high I are $\kappa < \gamma$ and $R < \gamma$ ²⁵, as shown in Fig 1.b. As the distance between the QEs decreases the R of the e-QE reduces, so I remains high for higher g values. This effect is easily visualized in Fig 1.d, where we plot the iso-contours of $I = 0.9$ for different values of d . Whereas the maximum g for $I > 0.9$ is about $g = 10\gamma$ when $d = 8.5 \cdot 10^{-2}\lambda$, this value increases to $g = 20\gamma$ when $d = 6.9 \cdot 10^{-2}\lambda$. In other words, the requirement for Q (i.e. $\kappa < \gamma$) remains unchanged and the R -reduction effect just enables high I for higher g values, which is not particularly interesting. Therefore, the implementation of the two-

QE system does not provide any practical advantages (in terms of Q and g) with respect to the single-QE. For the three distances, Fig. 1.f confirms the excellent agreement for I values obtained from equation (1) and from numerical simulations of the two-QE system (see methods).

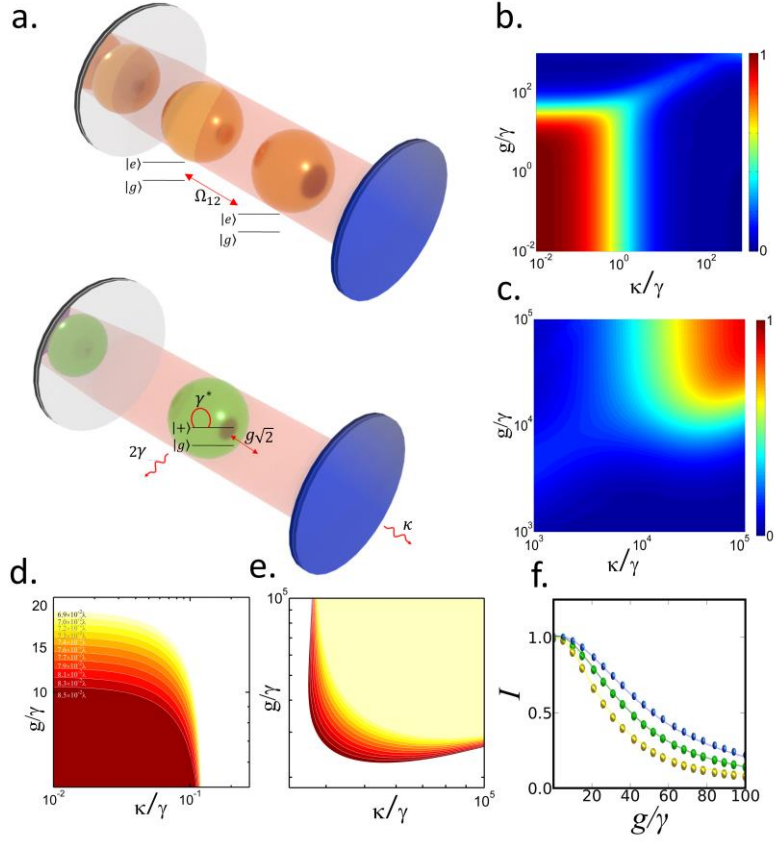


Figure 1. (a) The two interacting Qes with γ coupled to the cavity field with g are equivalent to a single QE with 2γ coupled to the cavity with $\sqrt{2}g$, each sphere represents a single two-level-system. Indistinguishability of the effective QE versus the normalized κ and g in the (b) incoherent regime, and (c) coherent regime. Contour map of regions with $I > 0.9$ for different distances between the emitters from $d = 6.9 \cdot 10^{-2}\lambda$ to $d = 8.5 \cdot 10^{-2}\lambda$ (d) incoherent regime and (e) coherent regime. (f) Indistinguishability versus normalized g for $d = 7.2 \cdot 10^{-2}\lambda$ (yellow), $d = 7 \cdot 10^{-2}\lambda$ (green) and $d = 6.9 \cdot 10^{-2}\lambda$ (blue); solid lines calculated using equation (1); coloured dots obtained from numerical integration of the Lindblad equation with two QEs.

In the coherent regime the conclusions are roughly similar. Within the range where g is close to the strong coupling condition, the (e-QE)-cavity system is equivalent to an effective emitter²⁵ with decay rate $2\gamma + R$. Here the condition for high I is $R > \gamma$ ²⁵, as shown in Fig 1.c. Same as before, reducing d decreases R , requiring higher g for high I . Fig 1.e shows the same iso-contours as Fig 1.d in the coherent regime. The $I > 0.9$ region narrows upwards as d decreases due to the same R reduction effect. Thus, in the coherent regime the two-QE system impose stronger restrictions than the single QE, since it demands higher g

values for getting high I . Therefore, the two-QE interface does not provide any advantage for high I in terms of cavity requirements, in the incoherent or coherent regimes. However, an extended exploration over systems with larger number of coupled emitters can be relevant. As we will show next, exploiting the cooperative behavior of optimized systems with more than 2 emitters can provide benefits in terms of I .

LARGER SYSTEMS

We showed before that for a set of interacting 2-level quantum systems in the incoherent regime the dynamics are described by a population transfer between the subsystems with effective transfer rates R . As an example, for a single QE coupled to a single-mode cavity field the evolution of the system reduces to the following rate equations²⁵:

$$\begin{pmatrix} \dot{P}_{QE} \\ \dot{P}_C \end{pmatrix} = \begin{pmatrix} -(\gamma + R) & R \\ R & -(\kappa + R) \end{pmatrix} \begin{pmatrix} P_{QE} \\ P_C \end{pmatrix} \quad (2)$$

Where P_{QE} is the population of the QE, P_C is the population of the cavity and $R = \frac{4g^2}{\Gamma}$. As it is described in the Methods section, I is obtained from the solution of (2) via the quantum regression theorem (QRT). Since QRT computation is an iterative process, it may be useful to study the dynamic stability of the characteristic equation of (2) to find any kind of relation with I . For this purpose, we have defined the degree of stability ($\bar{\theta}$) by measuring the speed of divergence of the characteristic equation of (2) (see methods). After some algebra, we have found a direct relationship between $\bar{\theta}$ and I (see equations (13) and (14) in Methods). This means that we can derive analytic expressions of I for arbitrary large system without having to compute the ne-G. Instead, we obtain I from the determinant $\bar{\Delta}$ and the trace τ of (2), which significantly simplifies the problem, specially for more complicated systems (like the ones with more than 2 emitters). This finding can be expressed as:

$$\bar{\theta} = I = \frac{\bar{\Delta}}{\tau} = \frac{\gamma + \frac{\kappa R}{\kappa + R}}{\kappa + 2R + \gamma} \quad (3)$$

Where $\bar{\Delta}$ is the normalized determinant (see Methods). In the same way than I , if κ increases, $\bar{\theta}$ decays at different rates depending on R . The alternative interpretation of I shown in Eq (3) provides some hints to find a way of keeping high I with higher κ values (i.e. to reduce the Q of the cavity). For the case of a single QE-cavity system the decay of $\bar{\theta}$ with κ can be tuned by changing R . If we include more QEs (or,

in general, more subsystems) we have additional transfer rates that may help even more to reduce the cavity Q . The additional transfer rates will show up in the off-diagonal terms of the rate equations, giving additional terms in Δ which can lead to new paths to improve the reduction of $\bar{\theta}$ with κ . This approach can be illustrated with the cascaded-cavities scheme²⁶. This system considers a single QE coupled to a cavity which at the same time is coupled to a second cavity. In the incoherent regime the dynamics follows the rate equations²⁶:

$$\begin{pmatrix} \dot{P}_{QE} \\ \dot{P}_{C1} \\ \dot{P}_{C2} \end{pmatrix} = \begin{pmatrix} -(\gamma + R_1) & R_1 & 0 \\ R_1 & -(\kappa_1 + R_1 + R_2) & R_2 \\ 0 & R_2 & -(\kappa_2 + R_2) \end{pmatrix} \begin{pmatrix} P_{QE} \\ P_{C1} \\ P_{C2} \end{pmatrix} \quad (4)$$

Where P_{C1} is the population of the first cavity, P_{C2} is the population of the second cavity, κ_1 is the decay rate of the first cavity, κ_2 is the decay rate of the second cavity, R_1 is the transfer rate between the QE and the first cavity, and R_2 is the transfer rate between the first and second cavities. In this case we have one more degree of freedom (R_2) than in the single QE-cavity system. Therefore, by adjusting R_1 and R_2 we can tune the decay of the stability with κ in a more efficient way. Fig 2.c shows a quantitative example of this improvement. While with the single QE-cavity system I decreases below 0.5 for $\kappa = \gamma$, the cascaded-cavities scheme can maintain $I > 0.5$ up to $\kappa_2 = 100\gamma$ when setting the right R_1 and R_2 values (i.e. setting the cavity mode volume, V_{eff} , and Q).

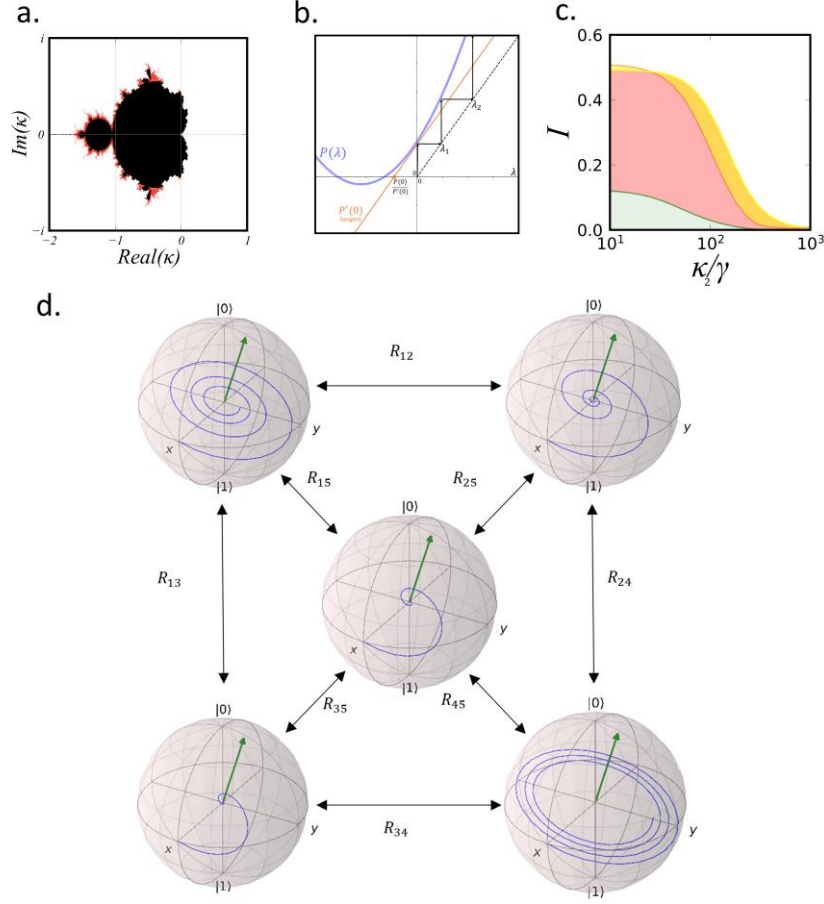


Figure 2. (a) κ -parameter space of the stability of rate equations of a single QE system coupled to a cavity. Black dots correspond to bounded points while the gradient colors represent the degree of stability. (b) Characteristic equation of (2) (blue line); tangent line with slope $P'(0)$. The cut of the tangent line with the x-axis is given by $\frac{P(0)}{P'(0)}$. The arrows indicate consecutive λ_n values of the iteration process. (c) Indistinguishability versus normalized κ_2 for $g_1 =$ (green), 2γ (red) and 3γ (yellow). (d) Bloch-spheres of the five-QE system with population rate transfers R_{ij} between each subsystem.

Therefore, adding more subsystems (emitters and/or cavities) provide additional paths to maintain the stability and therefore relax the cavity requirements for high I . Accordingly, now we study the case of a cluster of five QEs coupled to a single-mode cavity field. With this scheme, we have 10 transfer rates (R_{ij}) that can be tuned by setting the relative distances between the QEs (see Fig 2.d), so we have enough parameters to perform a sufficiently complex optimization. Our aim now is to find the geometrical configuration of the QEs that provides the optimal set of R_{ij} that keep high I for high κ values. This goal involves an optimization task with 10 degrees of freedom, which is a highly non-trivial problem and computationally very time-consuming. Nevertheless, similar optimization problems have been recently solved using machine-learning methods^{23,42,43,44,45}. Using a similar approach, we have developed a

machine-learning scheme based on a hybrid NN-GA algorithm which is able to solve the optimization problem in very short computational times providing the best geometrical configuration for the emitters.

MACHINE LEARNING OPTIMIZATION

We consider five QEs with γ^* randomly positioned in a 2D-grid. All of them are coupled to a single-mode cavity field with the same coupling constant g and cavity decay rate κ . Each relative distance d_{ij} ($i, j = 1, \dots, 5$) between QEs leads to a dipolar interaction strength Ω_{ij} and modified decay rate γ_{ij} . Since this scheme requires solving a system of 144 coupled differential equations, we are not able to derive an analytic expression for I like in the 2-QE case. Instead, we numerically solve the Lindblad equation of the system and compute I via QRT. At each iteration we generate a vector ω with 5 random positions for the qEs and we calculate I via QRT for a fixed g and κ . The data set (ω, I) is then used to train the NN-GA algorithm which finds the optimal positions for maximum I for that g and κ . In Fig 3.a,b,c,d,e we report the obtained optimal geometries for $g = \gamma$ and $\kappa = 10\gamma, 50\gamma, 100\gamma, 500\gamma$ and 1000γ respectively. All these geometries provide perfect I ($I = 1$) with minimum distances $d_{ij} \sim 0.1\lambda$, a value compatible with experimental realizations^{34,35,36,37,38,39,40,41}. Each geometry leads to the right transfer rates R_{ij} between the subsystems for keeping the stability at the specific rates g and κ . For a fixed geometry, small changes in g and κ drastically reduce I . This is displayed in Fig 3.f, which shows I versus normalized g/γ and κ/γ for the optimal geometry obtained for $g = \gamma, \kappa = 10\gamma$. The plot shows a small “bubble” of high I at the $(g/\gamma, \kappa/\gamma)=(1,10)$ point, while in the neighbor regions of the bubble I reduces to 0. Fig 3.a,b,c,d,e also show the positioning tolerances for each QE for getting $I > 0.9$. The accuracy in the position is more or less critical depending on the specific QE and the (g, κ) values.

Within our scheme the realization of perfect I SPS with strong dissipative QEs is possible using well established photonic platforms. To verify this claim we performed 3D-FDTD simulations⁴⁶ of a point source placed at the antinode of a cavity-mode in a standard 2D-hexagonal SiN photonic crystal cavity (PCc). The V_{eff} and Q were obtained from the field profile (see Fig 3.g) and frequency analysis of the resonance. For a QE with $(\gamma, \gamma^*, \omega) = (160 \text{ MHz}, 400 \text{ GHz}, 400 \text{ THz})$ like color centers in diamond⁴⁷ we obtained $(g, \kappa) \approx (1, 100)$. The radius and distances between the holes of the PCc were set to 120 nm and 50 nm respectively, which is compatible with most fabrication techniques^{48,49,50}.

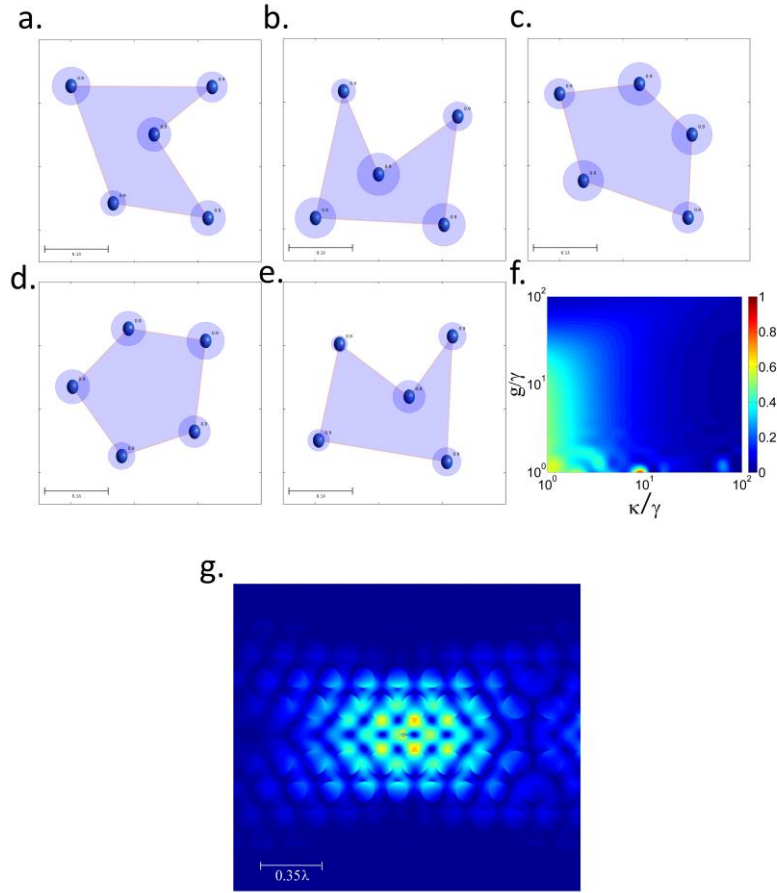


Figure 3. Optimal configuration of the 5-QEs system in a 2D plane for (a) $\kappa = 10\gamma$, (b) $\kappa = 50\gamma$, (c) $\kappa = 100\gamma$, (d) $\kappa = 500\gamma$, (e) $\kappa = 1000\gamma$. The circles around each QE position corresponds to the positioning tolerance for having $I > 0.9$. (f) Indistinguishability versus normalized κ and g for the optimized system shown in (a). (g) Field profile $|E|^2$ of the hexagonal PC-cavity-mode with a point source placed at the antinode.

A key point to evaluate for the experimental realization of our scheme is the nanoscale positioning approach for the deposition of the cluster of QDs. Novel positioning technologies have recently shown positioning accuracy at the nanometer level⁵¹. 30 nm positioning accuracy with GaAs QDs was reported using atomic force microscopy⁵². Confocal micro-photoluminescence can provide 10 nm positioning accuracy also with GaAs QDs as it was shown in [53]⁵³. 5 nm position accuracy was recently achieved with Bi-chromatic photoluminescence through a new image analysis software implementation⁵⁴. In-Situ lithography approaches have also shown promising results improving its position accuracy down to 30 nm⁵⁵. Pick-and-place approaches shown 38 nm positioning accuracy for Si vacancy centers transference to aluminum nitride waveguides, achieving 98% coupling efficiency^{56,57}. Therefore, according to tolerances shown in Figure 3.b, for the case of point defects in diamond, using pick-and-place positioning

we would have a standard deviation of 38 nm with a target of about 30 nm. This leads to 81% probability of successful deposition for a single QD. Successful deposition of the five QDs in place would have a probability of 32%. An experimental realization should require the fabrication of a large number of devices and checking for suitable candidates one by one. According to this, although our scheme could enable the experimental demonstration of certain quantum phenomena is still far from a high-scalable technology.

NON-IDENTICAL QUANTUM DOTS

So far, we have explored the theoretical performance of our scheme considering identical QDs without detuning Δ between the emitters. However, a more realistic analysis involves the evaluation of the effect of mismatching between the emission frequencies of the QDs. With this aim, we have incorporated a statistical detuning distribution to the system of 5 QDs in the configuration shown in Figure 3.b. We consider a normal distribution setting the mean equal to 0 and standard deviation $\sigma_n = n\gamma$, as shown in Figure 4.a. The Δ of each QD is set randomly according to the normal distribution. We start with the distribution $\sigma_1 = \gamma$, we set five random Δ for the QDs and compute I . Then we reset the random Δ according to the same distribution and compute again I , repeating this process 200 times and computing the average of all obtained values of I . We obtained the average value of I for the 20 different probability distributions $\sigma_n = n\gamma$ with $n = 1 \dots 20$, as shown in Figure 4.b.

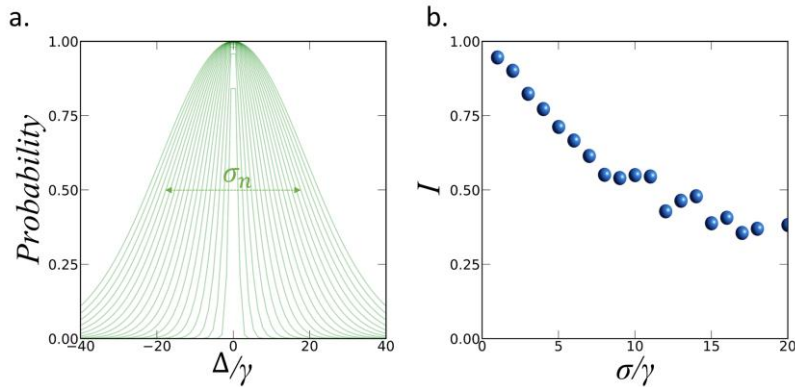


Figure 4. (a) Probability distributions with standard deviation σ_n for $n=1\dots 20$ for the normalized detuning values Δ/γ . At each iteration we set a random Δ value for each QD according the corresponding distribution. (b) Average value of the indistinguishability obtained for each of the 20 probability distributions.

As expected, the value of I reduces as the standard deviation of the distribution increases. For the distribution $\sigma_1 = \gamma$ the possible values for the Δ between the QDs range from -5γ to 5γ , leading to a

negligible reduction of I . On the opposite side, with $\sigma_{20} = 20\gamma$ the possible values of Δ range from -60γ to 60γ , giving a reduction of I of about 70%. According to these results, our scheme is able to maintain high $I > 0.75$ for normal distributions of emitters with standard deviation below 5γ , which includes frequency mismatching between the QEs of about 20γ . Therefore, the proposed system is a relatively robust platform for distributions of non-identical QDs according to recent experimental demonstrations⁵⁸.

Discussion

We have developed an analytical model for the estimation of the indistinguishability with two-QE interfaces with dephasing integrated in optical cavities. The model provides an analytical expression which relates the indistinguishability with the distance between the QEs and the parameters of the cavity. Through an alternative interpretation of the indistinguishability, we were able to estimate the behavior of systems including more QEs. Finally, we performed a numerical optimization of a 5-QE system coupled to a single cavity by a machine learning scheme. The results predict perfect indistinguishability with strong dissipative QEs in arbitrary low Q cavities. The proposed scheme provides a strategy for the realization of a source of perfect indistinguishable single photons at room temperature. The strategy presents significant challenges from the perspective of QD positioning process. Although the required accuracy in positioning may be still far from a real scalable technology it can be suitable for experimental demonstration of single photon operation with high indistinguishability. The ML approach used may provide insights for the optimization of different photonic structures for quantum information applications, like the reduction of quantum decoherence in clusters of coupled two-level quantum systems.

Methods

DIPOLE-DIPOLE COUPLING MODEL

After rotating wave approximation, the Hamiltonian for the two-QE system coupled the cavity single-mode field reads³⁰:

$$H = \Omega_{12}(\sigma_1^\dagger \sigma_2 + \sigma_1 \sigma_2^\dagger) + ig(a^\dagger(\sigma_1 + \sigma_2) - a(\sigma_1^\dagger + \sigma_2^\dagger)) \quad (5)$$

Where $\sigma_i/\sigma_i^\dagger$ are the lowering/rising operators of the QEs and a/a^\dagger the annihilation/creation operators of the cavity field. The terms associated with γ, γ^* and κ are described under Born-Markov approximation, so the evolution of the density matrix follows the Lindblad equation²⁹:

$$\frac{\partial \rho}{\partial t} = -i[H, \rho] + \sum_n (D_n \rho D_n^\dagger - \frac{1}{2}(D_n^\dagger D_n \rho + \rho D_n^\dagger D_n)) + 2\gamma \sum_{i \neq j} (\sigma_i \rho \sigma_j^\dagger - \frac{1}{2}(\sigma_j^\dagger \sigma_i \rho + \rho \sigma_j^\dagger \sigma_i)) \quad (6)$$

Where the D_n denotes the collapse operators: $\sqrt{\kappa}a$, and $\sqrt{\gamma^*} \sigma_i^\dagger \sigma_i$. We have assumed $kd \ll 1$ so the modified radiative decay rate is 2γ and $\Omega_{12} = \frac{3\gamma}{4(kd)^3}$ ³⁰. Without detuning between the QEs there is no coherent coupling between any state but the $\{|gg\rangle, |+\rangle\}$ set, so the Hamiltonian and Lindblad equation can be written as:

$$H = \Omega_{12}|+\rangle\langle +| + i\sqrt{2}g(a^\dagger \sigma_+ - a \sigma_+^\dagger)$$

$$\frac{\partial \rho}{\partial t} = -i[H, \rho] + \sum_n (D_n \rho D_n^\dagger - \frac{1}{2}(D_n^\dagger D_n \rho + \rho D_n^\dagger D_n)) \quad (7)$$

Where $\sigma_+ = \frac{\sigma_1 + \sigma_2}{\sqrt{2}}$ and now the D_n denotes the collapse operators: $\sqrt{\kappa}\hat{a}$, $\sqrt{2\gamma}\sigma_+$ and $\sqrt{\gamma^*}\sigma_+^\dagger\sigma_+$ ²⁹. The equations in (6) corresponds to the evolution of a system with a single effective QE with decay rate 2γ coupled to a single-mode cavity field with $\sqrt{2}g$. The degree of I is defined as²⁵:

$$I = \frac{\iint_0^\infty dt d\tau |\langle a^\dagger(t+\tau)a(t) \rangle|^2}{\iint_0^\infty dt d\tau \langle a^\dagger(t)a(t) \rangle \langle a^\dagger(t+\tau)a(t+\tau) \rangle} \quad (8)$$

Which can be computed numerically via QRT. Alternatively, to derivate an explicit formula for I we start from the following expressions of the master equation:

$$\begin{aligned} \frac{\partial \rho_{ee}}{\partial t} &= ig(\rho_{ec} - \rho_{ce}) - \gamma \rho_{ee} \\ \frac{\partial \rho_{cc}}{\partial t} &= ig(\rho_{ce} - \rho_{ec}) - \kappa \rho_{cc} \\ \frac{\partial \rho_{ec}}{\partial t} &= ig(\rho_{ee} - \rho_{cc}) - \left(\frac{\Gamma}{2} + \frac{3\gamma}{4(kd)^3}\right) \rho_{ec} \end{aligned} \quad (9)$$

In the incoherent regime we can apply adiabatic elimination of the coherences by setting $\frac{\partial \rho_{ec}}{\partial t} = 0$ ²⁵.

Substituting in (9) we obtain the rate equations (2) with the corresponding transfer rate R shown in (1).

We can now obtain the numerator of (8) by calculating the ne-G of the system from the equations of motion:

$$i \frac{\partial}{\partial t} \hat{G}^R(\tau) = i\delta(\tau)\hat{I} + [\hat{H} - i\hat{\Sigma}^R(0)]\hat{G}^R(\tau), \quad \hat{\Sigma}^R = \begin{pmatrix} (\gamma + \frac{\gamma^*}{2}) & 0 \\ 0 & \kappa/2 \end{pmatrix} \quad (10)$$

Where $\hat{G}^R(\tau)$ is the retarded $\hat{G}^R(\tau)$ and $\hat{\Sigma}^R$ the retarded self-energy. Following a similar procedure as in [25], the numerator in (8) can be substituted by

$$|\langle a^\dagger(t + \tau)a(t) \rangle|^2 = P_c^2(t) e^{-\tau(\kappa + 4g^2\Gamma/(\Gamma^2 + \frac{\gamma^2}{(ka)^6}))} \quad (11)$$

Solving equation (2) for P_c we can analytically solve (8), which gives the expression shown in (1).

LARGER SYSTEMS

We first obtain the characteristic polynomial of (2): $P(\lambda) = \lambda^2 + (\kappa + 2R + 1)\lambda + (\kappa R + \kappa + R)$, where we have set $\gamma = 1$. Then we set the iterative process $\lambda_{n+1} \Leftarrow P(\lambda_n)$ (from $\lambda = 0$) and check the stability in the parameter space (κ, R) . Fig 2.a shows the κ -parameter space of the stability of $P(\lambda)$ for a fixed R . Black dots in the complex plane correspond to κ values which the iteration stays bounded and doesn't diverge to infinity. White dots correspond to values which the iteration diverges to infinity at a maximum speed. Gradient colors correspond to values which the iteration diverge to infinity at different speeds. Our region of interest is the positive real line $\kappa \in \mathbb{R} > 0$. In this region the iteration diverges to infinity for all κ . We want to measure the speed of the divergence θ for each κ and R (i.e the number of iterations that takes the process to infinity). A good candidate to characterize this value is the slope of $P(\lambda)$ at $\lambda = 0$ (i.e. $P'(0)$). Since $P'(\lambda)$ grows monotonically with λ , $P'(0)$ uniquely determines θ (see Figure 2.b). In order to express θ in the decay rate units (λ units), we draw the tangent line to $P(\lambda)$ at $\lambda = 0$ (red line in Figure 2.b) and take the cut with the x-axis, which gives $\frac{P(0)}{P'(0)}$. With this definition θ reads:

$$\theta = \frac{P(0)}{P'(0)} = \frac{\kappa R + \kappa + R}{\kappa + 2R + 1} \quad (12)$$

In order to normalize θ we need to divide (12) by its maximum value θ_{max} . θ is maximum when $\kappa, R \ll 1$, therefore from (12) we have that $\theta_{max} = \kappa + R$. Then the normalized speed of divergence $\bar{\theta}$ is given by:

$$\bar{\theta} = \frac{\theta}{\theta_{max}} = \frac{\gamma + \frac{\kappa R}{\kappa + R}}{\kappa + 2R + \gamma} = I \quad (13)$$

Which matches the expression for I ²⁵. If we apply the same definition of $\bar{\theta}$ for the cascaded cavity system (equation (4)) we obtain:

$$\bar{\theta} = \frac{\kappa_1/2 + \frac{\kappa_2 R_2}{2(\kappa_2 + R_2)}}{\kappa_1/2 + \kappa_2 + \frac{3}{2}R_2} = I \quad (14)$$

Which again matches the expression for I^{26} after applying same approximations. Same way, for the two-emitter system $\bar{\theta}$ matches the I value shown in (1). Note that in general the $\frac{P(0)}{P'(0)}$ is equal to $\frac{\Delta}{\tau}$, where Δ is the determinant and τ is the trace of the rate equations matrix. Therefore, with this method we are able to obtain the analytic expression of I for any system from trivial operations in the rate equations, without the need of calculating the ne-G.

MACHINE LEARNING SCHEME

The Hamiltonian for the 5-QEs system coupled to a single-mode cavity field can be written as:

$$H = \sum_{i \neq j} \Omega_{ij} (\sigma_i^\dagger \sigma_j + \sigma_i \sigma_j^\dagger) + ig \sum_{i \neq j} (a^\dagger (\sigma_i + \sigma_j) - a (\sigma_i^\dagger + \sigma_j^\dagger))$$

With $i, j = (1, \dots, 5)$. The modified radiative decay rates γ_{ij} and the dipolar interaction strengths Ω_{ij} can be obtained from the Green's tensor of the system leading to³³:

$$\gamma_{ij} = \frac{3}{2} \{ \sin(kd_{ij})/kd_{ij} - 2(\cos(kd_{ij})/kd_{ij}^2) - \sin(kd_{ij})/kd_{ij}^2 \}$$

$$\Omega_{ij} = \frac{3}{4} \{ -\cos(kd_{ij})/kd_{ij} - 2(\sin(kd_{ij})/kd_{ij}^2) - \cos(kd_{ij})/kd_{ij}^2 \}$$

The evolution of the density matrix follows the Lindblad equation (6) substituting γ by γ_{ij} and adding the corresponding $\sqrt{\gamma^*} \sigma_i^\dagger \sigma_i$ operators. For each iteration the value of I is calculated by solving (6) numerically and computing (8) by QRT. As in each iteration a 12x12 matrix is diagonalized, the total time of each function evaluation can take several minutes. At the same time, a GA optimization may require 10^5 evaluations of the fitness function. If we directly use QRT for each evaluation, the optimization would require excessive computational times. Instead, in our approach we first generate a data set (ω, I) with the results obtained from 2000 iterations. With these data, we train a deep NN which learns to estimate the outcome of I for any possible set of random positions $\vec{\omega}$. Now, each time the GA creates a random vector ω , the evaluation of the fitness function obtains I from the estimation of the NN. This way, each evaluation takes just a few seconds. Through the iteration of cross-over and mutation, the GA finds the optimal configuration for maximizing I after a certain number of generations. Therefore, with our NN-GA scheme we reduce by two orders of magnitude the number of actual numerical simulations for the dataset.

The NN consists in a sequential layer model implemented in Keras module with the corresponding settings: Number of layers = 4; Neurons per layer = 200; input-dimension = 10; output dimension = 1; loss = mean square error; Epochs = 200; learning rate = 0.001; Batch size = 100; Number of samples = 2000. After the training with 2000 samples both loss and validation-loss converged to 10^{-3} , giving enough accuracy for the estimation of I and the optimization model. The Genetic Algorithm uses decimal representation for the genes, one point crossover and uniform mutation. The total initial population was set to 5000, the number of parents matings =2500, number of weights = 1000. We needed over 216 generations to find each optimal geometry.

Acknowledgments

We gratefully acknowledge financial support from the European Union's Horizon 2020 research and innovation program under grant agreement No. 820423 (S2QUIP) and CSIC Quantum Technology Platform PT-001y Agencia Estatal de Investigación (AEI) grant PID2019-106088RB-C31. We also thanks Dr. Ian Shlesinger for his contribution in the development of this work.

Author information

AFILIATIONS

Instituto de Micro y Nanotecnología, INM-CNM, Tres Cantos, Madrid, Spain: J.Guimbao, L.Sanchis, L.M.Weituschat, J.M. Llorens, P.A.Postigo.

The Institute of Optics, University of Rochester, Rochester, New York 14627, USA: P.A.Postigo.

CONTRIBUTIONS

J.G. wrote the manuscript developed the theory underlying the analytical formulas of the indistinguishability and machine learning algorithm. L.S. contributed to the development of the Machine Learning algorithm. L.M.W. and J.M.L. contributed to the development of the theory. P.A.P. supervised the project. All the authors revised the manuscript.

Competing interests

The authors declare not competing interests.

Data availability

Data underlying the results of this paper are available from the corresponding author upon request.

References

- [1] Monroe, C., Meekhof, D. M., King, B. E., Itano, W. M., & Wineland, D. J. (1995). Demonstration of a fundamental quantum logic gate. *Physical review letters*, 75(25), 4714.
- [2] Makhlin, Y., Schön, G., & Shnirman, A. (1999). Josephson-junction qubits with controlled couplings. *nature*, 398(6725), 305-307.
- [3] Politi, A., Cryan, M. J., Rarity, J. G., Yu, S., & O'brien, J. L. (2008). Silica-on-silicon waveguide quantum circuits. *Science*, 320(5876), 646-649.
- [4] Bunandar, D., Lentine, A., Lee, C., Cai, H., Long, C. M., Boynton, N., ... & Englund, D. (2018). Metropolitan quantum key distribution with silicon photonics. *Physical Review X*, 8(2), 021009.
- [5] Lago-Rivera, D., Grandi, S., Rakonjac, J. V., Seri, A., & de Riedmatten, H. (2021). Telecom-heralded entanglement between multimode solid-state quantum memories. *Nature*, 594(7861), 37-40.
- [6] Zhong, H. S., Wang, H., Deng, Y. H., Chen, M. C., Peng, L. C., Luo, Y. H., ... & Pan, J. W. (2020). Quantum computational advantage using photons. *Science*, 370(6523), 1460-1463.
- [7] Peruzzo, A., McClean, J., Shadbolt, P., Yung, M. H., Zhou, X. Q., Love, P. J., ... & O'brien, J. L. (2014). A variational eigenvalue solver on a photonic quantum processor. *Nature communications*, 5(1), 1-7.
- [8] Acosta, V. M., Bauch, E., Ledbetter, M. P., Santori, C., Fu, K. M., Barclay, P. E., ... & Budker, D. (2009). Diamonds with a high density of nitrogen-vacancy centers for magnetometry applications. *Physical Review B*, 80(11), 115202.
- [9] Juska, G., Dimastrodonato, V., Mereni, L. O., Gocalinska, A., & Pelucchi, E. (2013). Towards quantum-dot arrays of entangled photon emitters. *Nature Photonics*, 7(7), 527-531.
- [10] Gérard, J. M., Sermage, B., Gayral, B., Legrand, B., Costard, E., & Thierry-Mieg, V. (1998). Enhanced spontaneous emission by quantum boxes in a monolithic optical microcavity. *Physical review letters*, 81(5), 1110.

- [11] Hennessy, K., Badolato, A., Winger, M., Gerace, D., Atatüre, M., Gulde, S., ... & Imamoglu, A. (2007). Quantum nature of a strongly coupled single quantum dot–cavity system. *Nature*, *445*(7130), 896-899.
- [12] Wang, H., Duan, Z. C., Li, Y. H., Chen, S., Li, J. P., He, Y. M., ... & Pan, J. W. (2016). Near-transform-limited single photons from an efficient solid-state quantum emitter. *Physical Review Letters*, *116*(21), 213601.
- [13] He, Y. M., He, Y., Wei, Y. J., Wu, D., Atatüre, M., Schneider, C., ... & Pan, J. W. (2013). On-demand semiconductor single-photon source with near-unity indistinguishability. *Nature nanotechnology*, *8*(3), 213-217.
- [14] Somaschi, N., Giesz, V., De Santis, L., Loredò, J. C., Almeida, M. P., Hornecker, G., ... & Senellart, P. (2016). Near-optimal single-photon sources in the solid state. *Nature Photonics*, *10*(5), 340-345.
- [15] Borri, P., Langbein, W., Schneider, S., Woggon, U., Sellin, R. L., Ouyang, D., & Bimberg, D. (2001). Ultralong dephasing time in InGaAs quantum dots. *Physical Review Letters*, *87*(15), 157401.
- [16] Bayer, M., & Forchel, A. (2002). Temperature dependence of the exciton homogeneous linewidth in In 0.60 Ga 0.40 As/GaAs self-assembled quantum dots. *Physical Review B*, *65*(4), 041308.
- [17] Berthelot, A., Favero, I., Cassabois, G., Voisin, C., Delalande, C., Roussignol, P., ... & Gérard, J. M. (2006). Unconventional motional narrowing in the optical spectrum of a semiconductor quantum dot. *Nature Physics*, *2*(11), 759-764.
- [18] Bylander, J., Robert-Philip, I., & Abram, I. (2003). Interference and correlation of two independent photons. *The European Physical Journal D-Atomic, Molecular, Optical and Plasma Physics*, *22*(2), 295-301.
- [19] Mirin, R. P. (2004). Photon antibunching at high temperature from a single InGaAs/GaAs quantum dot. *Applied physics letters*, *84*(8), 1260-1262.
- [20] Dusanowski, Ł., Syperek, M., Misiewicz, J., Somers, A., Hoefling, S., Kamp, M., ... & Sęk, G. (2016). Single-photon emission of InAs/InP quantum dashes at 1.55 μm and temperatures up to 80 K. *Applied Physics Letters*, *108*(16), 163108.

- [21] Yu, P., Li, Z., Wu, T., Wang, Y. T., Tong, X., Li, C. F., ... & Wang, Z. M. (2019). Nanowire quantum dot surface engineering for high temperature single photon emission. *ACS nano*, *13*(11), 13492-13500.
- [22] Arakawa, Y., & Holmes, M. J. (2020). Progress in quantum-dot single photon sources for quantum information technologies: A broad spectrum overview. *Applied Physics Reviews*, *7*(2), 021309.
- [23] Guimbao, J., Sanchis, L., Weituschat, L., Manuel Llorens, J., Song, M., Cardenas, J., & Aitor Postigo, P. (2022). Numerical Optimization of a Nanophotonic Cavity by Machine Learning for Near-Unity Photon Indistinguishability at Room Temperature. *ACS Photonics*.
- [24] Guimbao, J., Weituschat, L. M., Montolio, J. L., & Postigo, P. A. (2021). Enhancement of the indistinguishability of single photon emitters coupled to photonic waveguides. *Optics Express*, *29*(14), 21160-21173.
- [25] Grange, T., Hornecker, G., Hunger, D., Poizat, J. P., Gérard, J. M., Senellart, P., & Auffèves, A. (2015). Cavity-funneled generation of indistinguishable single photons from strongly dissipative quantum emitters. *Physical review letters*, *114*(19), 193601.
- [26] Choi, H., Zhu, D., Yoon, Y., & Englund, D. (2019). Cascaded cavities boost the indistinguishability of imperfect quantum emitters. *Physical review letters*, *122*(18), 183602.
- [27] Saxena, A., Chen, Y., Ryou, A., Sevilla, C. G., Xu, P., & Majumdar, A. (2019). Improving indistinguishability of single photons from colloidal quantum dots using nanocavities. *ACS Photonics*, *6*(12), 3166-3173.
- [28] Ota, Y., Iwamoto, S., Kumagai, N., & Arakawa, Y. (2011). Spontaneous two-photon emission from a single quantum dot. *Physical review letters*, *107*(23), 233602.
- [29] Shlesinger, I., Senellart, P., Lanco, L., & Greffet, J. J. (2021). Time-frequency encoded single-photon generation and broadband single-photon storage with a tunable subradiant state. *Optica*, *8*(1), 95-105.
- [30] Shlesinger, I., Senellart, P., Lanco, L., & Greffet, J. J. (2018). Tunable bandwidth and nonlinearities in an atom-photon interface with subradiant states. *Physical Review A*, *98*(1), 013813.

- [31] Schilder, N. J., Sauvan, C., Sortais, Y. R. P., Browaeys, A., & Greffet, J. J. (2020). Near-resonant light scattering by a subwavelength ensemble of identical atoms. *Physical review letters*, 124(7), 073403.
- [32] Ficek, Z., Tanas, R., & Kielich, S. (1986). Cooperative effects in the spontaneous emission from two non-identical atoms. *Optica Acta*, 33(9), 1149-1160.
- [33] Lehmburg, R. H. (1970). Radiation from an N-atom system. I. General formalism. *Physical Review A*, 2(3), 883.
- [34] Hettich, C., Schmitt, C., Zitzmann, J., Kühn, S., Gerhardt, I., & Sandoghdar, V. (2002). Nanometer resolution and coherent optical dipole coupling of two individual molecules. *Science*, 298(5592), 385-389.
- [35] ogl, T., Campbell, G., Buchler, B. C., Lu, Y., & Lam, P. K. (2018). Fabrication and deterministic transfer of high-quality quantum emitters in hexagonal boron nitride. *ACS Photonics*, 5(6), 2305-2312.
- [36] Schröder, T., Trusheim, M. E., Walsh, M., Li, L., Zheng, J., Schukraft, M., ... & Englund, D. (2017). Scalable focused ion beam creation of nearly lifetime-limited single quantum emitters in diamond nanostructures. *Nature communications*, 8(1), 1-7.
- [37] Hail, C. U., Höller, C., Matsuzaki, K., Rohner, P., Renger, J., Sandoghdar, V., ... & Eghlidi, H. (2019). Nanoprinting organic molecules at the quantum level. *Nature communications*, 10(1), 1-8.
- [38] Bayer, M., Hawrylak, P., Hinzer, K., Fafard, S., Korkusinski, M., Wasilewski, Z. R., ... & Forchel, A. (2001). Coupling and entangling of quantum states in quantum dot molecules. *Science*, 291(5503), 451-453.
- [39] Kim, H., Kyhm, K., Taylor, R. A., Kim, J. S., Song, J. D., & Park, S. (2020). Optical shaping of the polarization anisotropy in a laterally coupled quantum dot dimer. *Light: Science & Applications*, 9(1), 1-10.
- [40] Takagahara, T. (2002). Excitonic Structures and Optical Properties of Quantum Dots. *Semiconductor Quantum Dots*, 59-114.
- [41] Senellart, P., Solomon, G., & White, A. (2017). High-performance semiconductor quantum-dot single-photon sources. *Nature nanotechnology*, 12(11), 1026-1039.

- [42] Sanchis, L., Cryan, M. J., Pozo, J., Craddock, I. J., & Rarity, J. G. (2007). Ultrahigh Purcell factor in photonic crystal slab microcavities. *Physical Review B*, 76(4), 045118.
- [43] Sanchis, L., Håkansson, A., López-Zanón, D., Bravo-Abad, J., & Sánchez-Dehesa, J. (2004). Integrated optical devices design by genetic algorithm. *Applied Physics Letters*, 84(22), 4460-4462.
- [44] Morgado-León, A., Escuín, A., Guerrero, E., Yáñez, A., Galindo, P. L., & Sanchis, L. (2011, June). Genetic algorithms applied to the design of 3D photonic crystals. In *International Work-Conference on Artificial Neural Networks* (pp. 291-298). Springer, Berlin, Heidelberg.
- [45] Marques-Hueso, J., Sanchis, L., Cluzel, B., de Fornel, F., & Martínez-Pastor, J. P. (2010). Genetic algorithm designed silicon integrated photonic lens operating at 1550 nm. *Applied Physics Letters*, 97(7), 071115.
- [46] Lumerical Inc.
- [47] Neu, E., Hepp, C., Hauschild, M., Gsell, S., Fischer, M., Sternschulte, H., ... & Becher, C. (2013). Low-temperature investigations of single silicon vacancy colour centres in diamond. *New Journal of Physics*, 15(4), 043005.
- [48] Englund, D., Faraon, A., Zhang, B., Yamamoto, Y., & Vučković, J. (2007). Generation and transfer of single photons on a photonic crystal chip. *Optics Express*, 15(9), 5550-5558.
- [49] Chang, W. H., Chen, W. Y., Chang, H. S., Hsieh, T. P., Chyi, J. I., & Hsu, T. M. (2006). Efficient single-photon sources based on low-density quantum dots in photonic-crystal nanocavities. *Physical review letters*, 96(11), 117401.
- [50] Clark, A. S., Husko, C., Collins, M. J., Lehoucq, G., Xavier, S., De Rossi, A., ... & Eggleton, B. J. (2013). Heralded single-photon source in a III–V photonic crystal. *Optics letters*, 38(5), 649-651.
- [51] Liu, S., Srinivasan, K., & Liu, J. (2021). Nanoscale Positioning Approaches for Integrating Single Solid-State Quantum Emitters with Photonic Nanostructures. *Laser & Photonics Reviews*, 15(10), 2100223.
- [52] K. Hennessy, A. Badolato, M. Winger, D. Gerace, M. Atatüre, S. Gulde, S. Fält, E. L. Hu, A. Imamoglu, *Nature* 2007, 445, 896-901.

- [53] S. M. Thon, M. T. Rakher, H. Kim, J. Gudat, W. T. M. Irvine, P. M. Petroff, D. Bouwmeester, *Appl. Phys. Lett.* 2009, 94, 11 1.
- [54] J. Liu, M. I. Davanco, L. Sapienza, K. Konthasinghe, J. V. De Miranda Cardoso, J. D. Song, A. Badolato, K. Srinivasan, *Rev. Sci. Instrum.* 2017, 88, 023116.
- [55] M. Gschrey, R. Schmidt, J.-H. Schulze, A. Strittmatter, S. Rodt, S. Reitzenstein, *J. Vac. Sci. Technol. B* 2015, 33, 2 021603.
- [56] Elshaari, A. W., Pernice, W., Srinivasan, K., Benson, O., & Zwiller, V. (2020). Hybrid integrated quantum photonic circuits. *Nature photonics*, 14(5), 285-298.
- [57] Wan, N. H. et al. Large-scale integration of near-indistinguishable artificial atoms in hybrid photonic circuits. Preprint at <https://arxiv.org/abs/1911.05265> (2019).
- [58] Arakawa, Y., & Holmes, M. J. (2020). Progress in quantum-dot single photon sources for quantum information technologies: A broad spectrum overview. *Applied Physics Reviews*, 7(2), 021309.